JOURNAL OF INTERDISCIPLINARY PERSPECTIVES

ISSN Print: 2984-8288, ISSN Online: 2984-8385
Vol. 4 No. 3, pp. 132-151, March 2026

Original Article

The Anatomy of Uncertain Terrains: Soil Topography Characterization and Discharge Analysis of the Baroro River Basin, Northern Philippines

Jericho A. Trio , ***Patricia Mae M. Clariño*** , ***Chris C. Guevarra***

Author Information:

University of the Philippines Los Baños, Laguna, Philippines

Correspondence:
jatrio@up.edu.ph

Article History:

Date received: December 24, 2025
Date revised: January 30, 2026
Date accepted: February 12, 2026

Recommended citation:

Trio, J., Clariño, P.M., & Guevarra, C. (2026). The anatomy of uncertain terrains: Soil topography characterization and discharge analysis of the Baroro River Basin, Northern Philippines. *Journal of Interdisciplinary Perspectives*, *4*(3), 132-151. https://doi.org/10.69569/jip.2025.818

Abstract. The Baroro River Basin in Northern Luzon is a critical hydrological feature providing irrigation and biodiversity services. However, the watershed faces severe vulnerabilities due to the interplay between high-discharge hydrological behaviors and anthropogenic pressures, specifically rapid Land Use and Land Cover (LULC) changes that fragment forest blocks and compromise soil stability. While socio-ecological baselines and local perceptions of degradation are well documented, there remains a lack of integrated quantitative modeling of the pedological and lotic processes on which human settlements depend. Existing studies do not adequately account for the physical feedback loops among soil properties, river discharge, and landscape fragmentation. This study used the Soil and Water Assessment Tool+ (SWAT+) in QGIS to simulate hydro-pedological trajectories from 1963 to 2063. The methodology integrated remote sensing with descriptive statistics to correlate variables such as Topographic Wetness Index (TWI), Soil Bulk Density (BD), and Soil Water Potential (SWP) against historical rainfall data. The analysis revealed the San Juan Anomaly, a 2–3 km zone of amplified TWI and sediment accumulation acting as a vital hydrological capacitor for riverine agriculture. Statistical modeling showed a decoupling between precipitation and discharge, with high upstream porosity (BD ≈ 0.69 g/cm^3) buffering storm runoff. However, a sharp divergence exists between the simulated restorative potential forest recovery and the observed reality of downstream urban compaction and soil densification. The basin demands a management paradigm that treats it as a single functional unit. Immediate policy interventions must zone the San Juan alluvial scar for sustainable agriculture to prevent infrastructure encroachment. Long-term strategies should prioritize deep pedological rehabilitation through upstream reforestation to reduce bulk density, thereby restoring carbon storage and flood-mitigation capacity.

Keywords: *Baroro River Basin; River pedology; River remote sensing; Soil taxonomy; Topographic wetness.*

The Baroro River Basin, situated in the montane environs of Northern Luzon, is a critical hydrological feature spanning approximately 19,432.50 hectares across six municipalities in La Union: San Gabriel, Bagulin, San Juan, Bacnotan, Santol, and San Fernando City (Lahoti et al., 2025). Topographically characterized by a dendritic structure and acute tributaries, the watershed drains from the foothills of the Cordillera Administrative Region (CAR) into the West Philippine Sea (Ramirez et al., 2019). While this system supports vital ecosystem

services, its physical configuration presents inherent vulnerabilities. The watershed experiences an average annual surface runoff of 2,426.63 mm, with significant peaks during typhoon seasons (Cruz et al., 2014). Consequently, the interplay between this high-discharge hydrological behavior and increasing land-use pressures creates a compelling need for a rigorous soil–water assessment to mitigate agricultural vulnerability and hydrological risks.

In terms of its ecosystem services, the Baroro River Basin is a vital resource for irrigation, domestic water supply, and biodiversity. However, anthropogenic pressures primarily driven by rapid land use and land cover (LULC) changes have placed the river basin within the margins of vulnerability (Almarines et al., 2024; Pulhin et al., 2024; Ramirez et al., 2022). The river system, in terms of its biodiversity and ecosystem integrity, has declined and become gravely fragmented by episodes of urban sprawl (Ramirez et al., 2019). The trajectory of the basin's degradation is rooted in historical shifts in land use. Early assessments by Ramirez et al. (2019) identified significant alterations to the watershed's landscape, characterized by the conversion of forest land to agricultural and built-up areas. These changes have led to severe forest fragmentation, compromising the watershed's hydrological functions and increasing susceptibility to hazards such as flooding and soil erosion. The fragmentation of continuous forest blocks into smaller, isolated patches has disrupted wildlife habitats and reduced the basin's capacity to regulate water flow effectively (Ramirez et al., 2022).

Building on these physical assessments, Ramirez et al. (2019) and Ramirez et al. (2022) emphasized the human dimension of these environmental changes. Their research demonstrates that local communities are keenly aware of the deterioration of ecosystem services. Using the "livelihood, income, forest condition, and ecosystem services" (LIFE) framework, these studies found that residents' perceptions closely align with scientific data on forest loss and water scarcity. Local knowledge confirms that the decline in forest cover has directly affected the availability of provisioning services, such as freshwater and raw materials, thereby threatening local livelihoods that depend on these natural resources.

The ecological consequences extend beyond the immediate loss of resources to broader climate implications. Pulhin et al. (2024) quantified the impact of LULC changes on the basin's carbon storage capacity. The study revealed a marked decline in carbon sequestration due to the reduction of forest cover for urban and agricultural expansion. Unlike other watersheds that may benefit economically from such conversions, the Baroro River Basin has incurred economic costs from these land-cover changes, underscoring the urgent need for site-specific management strategies to recover its carbon-stock potential (Pulhin et al., 2024). Furthermore, the dynamics between food production and ecosystem health present a critical challenge. Almarines et al. (2024) explored the trade-offs between bioproduction systems and habitat quality. While the basin remains relatively stable in terms of habitat quality compared to other watersheds, there is a discernible decline in food production, particularly in rice and corn yields. This suggests that current land management practices may be failing to balance the competing demands of food security and biodiversity conservation. The study highlights trade-offs and potential synergies, advocating spatial planning that integrates bioproduction with the maintenance of ecosystem services.

To manage these complex interactions, watershed thinking has emerged as a vital paradigm, advocating for boundary-crossing measures that treat the river basin as a single functional unit. This approach integrates biophysical dimensions to enhance watershed literacy and awareness of water cycles (Sammel & McMartin, 2014). However, operationalizing this holistic philosophy requires advanced spatial–temporal tools. Remote sensing and Geographic Information Systems (GIS) have become indispensable for translating watershed theory into practice, providing a lens for understanding river morphology, streamflow, and landscape discontinuities (Umar et al., 2018). In the context of changing land use, these technologies are essential for predicting erosion, nutrient runoff, and flooding susceptibility (Issac & Newell, 2025). Despite the availability of these technologies, current literature on the Baroro River Basin remains heavily skewed toward socio-ecological perspectives. Existing scholarship has documented habitat fragmentation, agroecosystems, and local perceptions of ecosystem services, revealing that resident observations align with historical land-use shifts (Almarines et al., 2024; Pulhin et al., 2024; Ramirez et al., 2019; Ramirez et al., 2022). However, a critical research gap exists: while the anthropocentric and socio-ecological baselines are well established, there is no integrated quantitative modeling approach for the pedological and lotic (flowing water) behaviors on which these human settlements depend. The existing body of work does not sufficiently account for the physical feedback loops between soil properties and river discharge under varying climatic conditions.

The primary justification for a soil assessment is the alarming rates of land-cover change observed in the watershed. Research indicates that the basin has undergone significant landscape fragmentation, with continuous forest blocks converted into agricultural land and built-up areas (Ramirez et al., 2022). This transition removes the protective vegetative cover that stabilizes soil, making the terrain highly susceptible to erosion. Without a detailed soil assessment, it is impossible to identify high-risk erosion zones or accurately quantify sediment yield. Understanding soil stability is crucial because excessive sedimentation can silt up river channels, reduce the carrying capacity of waterways, and exacerbate flood risks for downstream communities (Ramirez et al., 2019). Furthermore, assessing soil health is vital for agricultural planning, as declining soil fertility directly affects the livelihoods of farmers who depend on the basin for crop production (Ramirez et al., 2022). A water assessment is indispensable to monitor the hydrological response to these landscape changes. The alteration of the basin's vegetative cover disrupts the natural water cycle, potentially leading to lower aquifer recharge rates and reduced streamflow during dry periods (Almarines et al., 2024). Understanding the basin's water quantity dynamics is essential for climate resilience. As climate change alters precipitation patterns, baseline data on streamflow and water retention are required to model future scenarios and develop infrastructure that can withstand extreme weather events (Pulhin et al., 2024). A scientific assessment of soil and water provides the empirical evidence needed to validate these local perceptions and inform policy. It enables decision-makers to move beyond reactive measures and implement integrated watershed management strategies that balance economic development with ecological preservation.

This study aims to bridge this gap by prioritizing the hydro-meteorological and pedo-topographic determinants of river basin integrity. As Lal (2015) argues, the feasibility of agricultural production is strictly governed by soil physical properties; forcing high-water-demand crops into poorly drained soils leads to systemic waterlogging and degradation. Similarly, the river's lotic behavior serves as a non-negotiable blueprint for built environments. Ignoring natural drainage patterns and river physics during construction significantly amplifies the risk of hydrological disasters (Wohl, 2014). This research introduces a methodological approach for the Baroro River Basin by linking Soil and Water Assessment Tool+ (SWAT+) simulations with remote sensing–derived pedological indicators. The findings aim to contribute significantly to interdisciplinary environmental decision-making, offering a predictive framework that ensures agricultural and urban developments operate within the safe physical boundaries of the river system.

Methodology

Study Site

The Baroro River Basin lies between latitudes 16°36'59" N to 16°44'7" N and longitudes around 120°20' E. Elevations range dramatically from sea level at the coastal outlet to 1,415 meters above sea level in the upstream headwaters near Barangay Lon-oy in San Gabriel. Climatically, the region falls under Type I in the Modified Coronas Classification, with a pronounced dry season from November to April and a wet season dominated by the southwest monsoon (Lahoti et al., 2025). Annual precipitation averages 2,277 mm, concentrated in the wet months with peaks > 700 mm in August (Cruz et al., 2014).

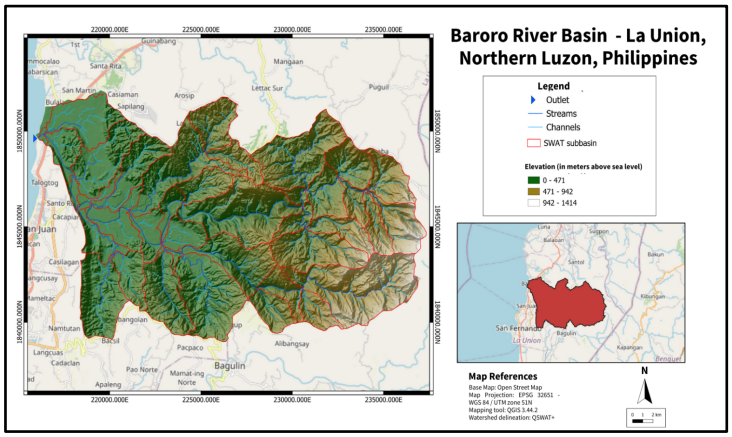

Figure 1. *The Baroro River Basin, La Union, Northern Philippines*
(Map created via QGIS projected at EPSG 32651; watershed delineation via SWAT+.)

Research Design

A hydrological research design integrates both descriptive and simulation-based methodologies to model complex watershed processes effectively. In the context of the Soil and Water Assessment Tool (SWAT+) in QGIS, the research design typically begins with a descriptive phase. This stage focuses on accurately characterizing the study area's physical reality by aggregating spatial datasets, such as Digital Elevation Models (DEMs), land-use maps, and soil properties. The integration of QGIS with SWAT+ streamlines this workflow, allowing researchers to precisely describe catchment features and define Hydrological Response Units (HRUs) based on observed environmental variables. In this phase, descriptive statistics such as frequency distribution tables, measures of central tendency, and measures of dispersion are considered (Chawanda et al., 2020). By coupling these designs, researchers can validate the model against the historical data described, providing predictive insights for watershed management.

Data Sources

Table 1. *Roster of QGIS Tools and Plugins Considered in the Conduct of the Output*

Geographical Data	Format	Resolution	Year Availability	Data Source
Baroro Watershed Digital Elevation Model	Raster (.tiff)	30 meters	2025	Copernicus (Extracted from CodeStudio - Google Earth Engine)
Baroro Watershed Land Cover Map	Raster (.tiff), Vector (.shp)	30 meters	2020	www.gadm.org www.geoportal.gov.ph
Soil Water Potential (in kPa)	Raster (.tiff); Extracted Vector (.shp) via Google Earth Engine	250 meters	2018	https://developers.google.com/earth-engine/datasets/catalog/OpenLandMap_SOL_SOL_WATERCONTENT-33KPA_USDA-4B1C_M_v01
Soil Bulk Density (in g/cm³)	Raster (.tiff); Extracted Vector (.shp) via Google Earth Engine	250 meters	2018	https://developers.google.com/earth-engine/datasets/catalog/OpenLandMap_SOL_SOL_BULKDENS-FINEEARTH_USDA-4A1H_M_v02
Soil Taxonomy (USDA)	Raster (.tiff); Extracted (.shp) via Google Earth Engine	250 meters	2018	https://developers.google.com/earth-engine/datasets/catalog/OpenLandMap_SOL_SOL_GRTGROUP_USDA-SOILTAX_C_v01
Precipitation Data	Text File	—	January 1963 – October 2025	Philippine Weather Stations

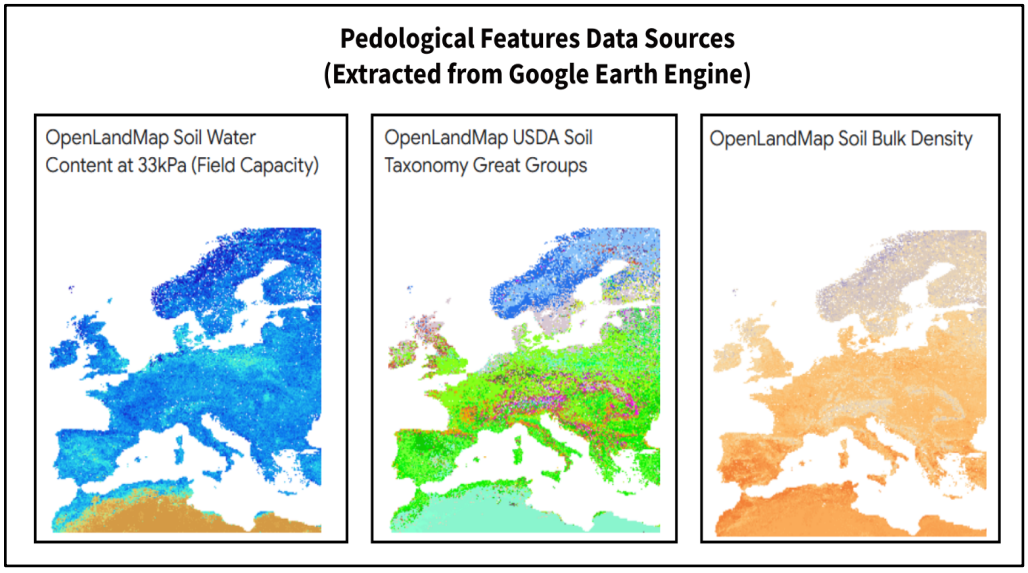

Figure 2. *Pedological Features Data Sources Extracted from Google Earth Engine*

Statistical and Remote Sensing Software

QGIS

QGIS (Quantum Geographic Information System) provides an open platform for geospatial analysis of watersheds and for river remote sensing. The authors of this study recognized that each QGIS version offers a distinct set of tools for conducting geographical surveys and assessments; therefore, three versions were considered: QGIS 3.36.3, QGIS 3.40.8, and QGIS 3.44.2. The following tools were placed into the utility and their corresponding objectives for accomplishing this research endeavor:

Table 2. *Roster of QGIS Tools and Plugins Considered in the Conduct of the Output*

Plugins and Tools	Objective	QGIS 3.36.3	QGIS 3.40.8	QGIS 3.44.2
Clipper	Clipping function in a similar shapefile through polygon line selection as a clipping feature.		■	■
MapTiler	Base maps using OpenStreetMap data by vector tiles served from MapTiler Cloud.		■	■
QSWAT 2.0.3	For soil and water assessment.	■	■	
QSWAT+	For soil and water assessment.		■	■
SAGA-Next Gen Fill Sinks Tool (Wang and Liu)	Ascertains a continuous downward slope for hydrological analysis.	■	■	■
SAGA-Terrain Analysis	For capturing the topographic wetness index.		■	■

Legend: ■ Presence of tool/ plug-in.

RStudio 4.5.1 and JASP 0.18.3

For statistical analysis and descriptive summaries, the proponents of this study used RStudio 4.5.1 and JASP 0.18.3. RStudio plugins in use were ggplot2 for graphical representation, Sim.DiffProc for Geometric Brownian Motion, and hydroGOF for diagnostic checks of the SWAT model. For the feasibility of descriptive summary statistics, JASP 0.18.3 was placed into utility– this included quick analysis for measures of spread and measures of central tendency.

Terrain and Hydrological Metrics

Soil Bulk Density

According to Arkhangelskaya and Lukyashchenko (2018), soil bulk density (BD) is a critical physical parameter calculated as the mass of dry soil divided by its total volume, accounting for both solid particles and pore spaces. BD is widely utilized to evaluate the structural integrity and compaction levels of soil. An increase in bulk density typically indicates reduced porosity, which reduces hydraulic conductivity and hampers root development, thereby increasing surface runoff. In contrast, lower bulk density values suggest ample pore space, creating an environment conducive to water retention.

Soil Water Potential

Soil water potential (SWP) refers to the energy status of soil moisture in comparison to a standard reservoir of pure water. As noted by Hillel (2003), this energy differential is the primary force governing the velocity and direction of hydraulic movement, with water naturally migrating from high-potential zones (wet) toward low-potential zones (dry). Understanding SWP is essential for accurately modeling evapotranspiration rates and assessing water accessibility for plant uptake.

Topographic Wetness Index

The Topographic Wetness Index (TWI) is a spatial analysis metric used to determine how terrain features influence hydrological distribution. By utilizing DEMs in platforms such as SAGA or QGIS, researchers can estimate soil moisture patterns and identify areas prone to saturation and runoff. Established by Beven and Kirkby (1979), the TWI model operates under the assumption of steady-state conditions, positing that the local hydraulic gradient is approximately equal to the terrain slope.

Watershed Delineation

The HRU definition utilized for the watershed delineation in this study employed a multiple-threshold approach to optimize the balance between spatial detail and computational efficiency. According to the theoretical documentation of the Soil and Water Assessment Tool (SWAT), HRUs represent unique combinations of land use, soil characteristics, and slope classes that dictate the hydrological behavior of the subbasin (Shawul et al., 2013). To avoid excessive model complexity caused by negligible spatial units, this study adopted a hierarchical filtration method consistent with established modeling protocols (Lee et al., 2021; Park et al., 2019).

The delineation process applied a strict percentage-based elimination sequence. Initially, a 10% threshold was established for land use coverage: any specific land use category occupying less than 10% of the subwatershed area was deemed hydrologically insignificant and subsequently removed, with its area reallocated proportionally among the remaining dominant land use types to preserve the total subwatershed area. Following this, a secondary 20% threshold was applied to the soil layer. Within the remaining land use classes, any soil taxon covering less than 20% of the area was eliminated and redistributed among the prevailing soil groups. Finally, a 10% threshold was imposed on slope classes (Aloui et al., 2023).

This ensured that minor topographic variations did not cause the basin to fragment into unmanageable micro-units. By ignoring these minor spatial components, the model reduces the total number of HRUs to a manageable number while maintaining the watershed's macroscopic physical properties necessary for accurate streamflow simulation (Raghuwanshi et al., 2006). This "lumping" technique allows the simulation to account for spatial heterogeneity without the computational burden of mapping every minor landscape feature one-to-one (Setegn et al., 2008).

Geometric Brownian Motion

To address the inherent uncertainty and temporal variability of landscape evolution over a century-scale timeline, this study utilized Geometric Brownian Motion (GBM) to simulate long-term trajectories for pedo-topographic metrics. While these parameters are often treated as static in short-term modeling, a hundred-year simulation requires accounting for stochastic fluctuations driven by environmental stressors, land cover changes, and climatic anomalies. GBM, a continuous-time stochastic process, is particularly suitable for these natural variables because it ensures that the simulated values remain strictly positive, a physical requirement for soil and topographic properties, while capturing the random drift and shock inherent in natural systems (Allen, 2007). The simulation posits that the value of a pedo-topographic metric X at time t evolves according to a stochastic differential equation

(SDE). This approach assumes that the percentage change in the metric is independent of its current value, allowing for exponential growth or decay perturbed by random noise.

$$dX_t = \mu X_t dt + \sigma X_t dW_t \quad (1)$$

Where:

x_t represent the pedo-topographic metric at time t
μ is the drift coefficient, representing the expected deterministic trend
σ is the volatility coefficient, representing the magnitude of environmental fluctuations
dW_t is the increment of a Brownian motion representing random noise

Through the implementation of Itô's Lemma (Bressloff, 2024), the following arrangements were pursued to project the metrics over the 100 years (1963 – 2063):

$$X_t = X_0 \, exp\,[(\mu - \frac{\sigma^2}{2})t + \sigma W_t] \quad (2)$$

Where:

x_0 represent the initial value at time t

This formula generates multiple realization paths, providing a probabilistic envelope of possible future soil and terrain conditions rather than a single deterministic outcome. This stochastic framework aligns with methodologies in environmental systems analysis where predictive uncertainty is substantial (Herrera et al., 2022). By shocking the initial parameters derived from the descriptive phase, the model robustly tests the resilience of the watershed's hydrological response across varying theoretical river-basin scenarios.

Descriptive Analysis

In soil remote sensing, calculating the central tendency of spectral signatures helps researchers identify the dominant properties of land-cover classes, facilitating the accurate delineation of HRUs (Lillesand et al., 2015). Without robust estimates of mean values, the calibration of satellite-derived datasets against in situ observations would lack a reliable baseline, potentially introducing systematic bias into subsequent hydrological models. Equally critical are measures of spread, such as standard deviation and the coefficient of variation, which quantify the heterogeneity inherent in natural landscapes. In river basin analysis, the average condition rarely dictates extreme events; rather, it is the variance in precipitation and flow data that characterizes a watershed's vulnerability to flooding or drought (Gutmann et al., 2014). For soil mapping, the standard deviation serves as a proxy for spatial uncertainty. A high degree of dispersion within a satellite pixel's value suggests a mix of soil types or vegetation cover (sub-pixel heterogeneity), warning the analyst against treating the area as a uniform entity (Crow et al., 2012). By rigorously applying these summary statistics, researchers can distinguish genuine environmental signals from random noise, ensuring that the physical reality described in the study is statistically valid before stochastic simulations are applied, as in the case of Geometric Brownian Motion.

Bivariate Analysis

The Pearson correlation coefficient is computed by normalizing the covariance of two quantitative variables by their product of standard deviations. This formulation ensures the result is dimensionless, allowing for the comparison of relationships between variables with different units. The formula is expressed as:

$$r = \frac{\sum_{i=1}^{n} (x_i - \underline{x})(y_i - \underline{y})}{\sqrt{\sum_{i=1}^{n} (x_i - \underline{x})^2}\sqrt{\sum_{i=1}^{n} (y_i - \underline{y})^2}} \quad (3)$$

Where:

x_i and y_i are the individual sample points from two data sets
$\underline{x}$ and $\underline{y}$ represent the sample means of the respective data sets
n is the sample size

Diagnostic Checks

Nash-Sutcliffe Efficiency

The NSE is a normalized metric used to evaluate the predictive power of hydrological models. It operates by comparing the variance of the model's errors with that of the observed data. The score ranges from -∞ to 1, where

1 indicates a perfect correlation between the model and reality. According to guidelines established by Moriasi et al. (2007), a model is generally considered satisfactory if it achieves an NSE score greater than 0.50. The NSE is implemented under the following equation:

$$NSE = 1 - \frac{\sum_{i=1}^{n} (Q_{obs,i} - Q_{sim,i})^2}{\sum_{i=1}^{n} (Q_{obs,i} - \underline{Q}_{obs})^2} \quad (4)$$

Where:

$Q_{obs,i}$ is the observed flow at time step i
$Q_{sim,i}$ is the simulated at time step i
$\underline{Q}_{obs}$ is the mean of the observed flow data
n is the total number of observations

Kling-Gupta Efficiency

Rather than relying on a single measure of error, the *Kling-Gupta Efficiency* (KGE) is a composite index that aggregates three distinct components: correlation, bias, and variability. It evaluates performance by measuring the geometric distance between the model's output and an optimal benchmark point. This approach provides a balanced view of how well the simulation mimics the properties of the observed data.

$$KGE = 1 - \sqrt{(r-1)^2 + (\alpha-1)^2 + (\beta-1)^2} \quad (5)$$

Where:

r is the Pearson correlation coefficient between observed and simulated data
α is the variability ratio
β is the Bias ratio

Percent Bias

Percent Bias (PBIAS) assesses the systematic error in a simulation by calculating the average percentage difference between modeled results and observed records. This metric specifically highlights the model's tendency to skew high or low. A positive PBIAS indicates that the model underestimates values (the observation exceeds the simulation). At the same time, a negative PBIAS suggests that the model is overestimating values (the observation is less than the simulation).

$$PBIAS = \frac{\sum_{i=1}^{n} (Q_{obs,i} - Q_{sim,i}) \cdot 100}{\sum_{i=1}^{n} Q_{obs,i}} \quad (6)$$

Where:

$Q_{obs,i}$ is the observed flow at time step i
$Q_{sim,i}$ is the simulated at time step i

Theoretical and Estimated Standard Deviation

Comparing theoretical and estimated standard deviations is a critical validation step that confirms that the simulation's realized volatility aligns with the historical input parameters. Specifically, the theoretical standard deviation refers to the target volatility parameter (σ) initially input into the Geometric Brownian Motion equation, whereas the estimated standard deviation is derived from the log-returns of the generated series. For a successful model, the output (estimated) volatility should closely mirror the input (theoretical) volatility.

$$\sigma_{estimated} = \sqrt{\frac{1}{n-1} \sum_{i=1}^{n} (R_i - \underline{R})^2} \quad (7)$$

Where:

n is the total number of time steps (100 years)
R_i is the log-return at time t_i
R is the mean of log returns

Kolmogorov-Smirnov (K-S) Normality Test Statistic

The Kolmogorov-Smirnov (K-S) normality test utilizes the statistic (D)to measure goodness-of-fit by quantifying the maximum distance between the Empirical Cumulative Distribution Function (ECDF) of the simulated log-returns and the Cumulative Distribution Function (CDF) of a theoretical normal distribution. The p-value

determines the significance of this test; a result greater than 0.05 suggests the data does not differ significantly from a normal distribution, thereby validating the GBM assumption.

$$D = sup_x |F_n(x) - F(x)| \quad (8)$$

Where:

D is the Kolmogorov-Smirnov statistic
sup_x is the supremum (maximum absolute difference)
$F_n(x)$ is the empirical cumulative distribution function of standardized log returns
$F(x)$ is the theoretical cumulative distribution function of the standard normal distribution

Lag-1 Autocorrelation

The lag-1 autocorrelation metric (r_i) measures the linear dependence between a variable's value at time t and its value at the previous time step t-1, quantifying the memory or persistence of the soil property. An autocorrelation coefficient close to zero suggests the data series behaves like white noise or a random process, indicating no substantial linear correlation between sequential data points (Box et al., 2015).

$$r_i = \frac{\sum_{i=1}^{n} (X_t - \underline{X})(X_{t+1} - \underline{X})}{\sum_{i=1}^{n} (X_t - \underline{X})^2} \quad (9)$$

Where:

X_t is the value of the pedo-topographic metric at time t
X_{t+1} the value of the metric at time t + 1 (the time ahead)
$\underline{X}$ is the mean of the time series

Data Cleaning

Prior to integrating spatial and temporal datasets into the SWAT+ environment, a rigorous data-cleaning protocol was implemented to ensure hydrological consistency of the Baroro River Basin model. The preprocessing phase began with standardizing spatial inputs (DEM, land cover, and soil maps) in QGIS 3.44.2. All raster datasets were reprojected to a uniform Coordinate Reference System (CRS) and resampled to ensure pixel alignment, thereby preventing geometric errors during watershed delineation. For the historical precipitation data (1963–2023), the time series was subjected to diagnostic checks for continuity. Statistical screening of the pedological metrics was conducted in RStudio 4.5.1, using boxplots and standardized z-scores to identify and remove outliers that deviated significantly from USDA soil taxonomy ranges. The "10/20/10" HRU threshold rule served as a filter, systematically eliminating negligible land use and soil fragments to reduce computational noise and enhance the model's computational efficiency without compromising the catchment's descriptive physical reality.

Ethical Considerations and Limitations

Ethical considerations centered on the responsible use of open-access geospatial data; all secondary datasets, including SRTM Digital Elevation Models and USDA soil taxonomies, were rigorously attributed to their respective agencies to uphold intellectual property rights and data-use policies. As the research design was purely computational and did not involve human subjects, the ethical scope was defined by data fidelity and the honest disclosure of methodological constraints. Regarding limitations, the authors acknowledge the inherent simplifications imposed by the SWAT+ environment. The application of the "10/20/10" HRU threshold rule, while essential for computational efficiency, inevitably aggregates minor land use and soil features, potentially masking micro-scale hydrological responses. Furthermore, relying on arithmetic mean imputation to address gaps in the historical precipitation record (1963–2023) introduces uncertainty into long-term rainfall-runoff simulations. It is critical to recognize that the study's results are based on a computational and simulation-based research design. The results should not be construed as dogmatic but rather as possible scenarios for future management of the Baroro River Basin.

Results and Discussion

Watershed Profile

The SWAT+ delineation of the Baroro Watershed identified a complex drainage network comprising 43 subbasins and 417 individual channel segments (reaches). The spatial distribution of these channels exhibits distinct heterogeneity (Figure 3). High drainage density is observed in the central-eastern upland zones (approx. coordinates 230,000 E, 1,640,000 N), particularly within the Bagulin and San Gabriel subbasins, which encompass 60% of the total dendritic network. Moving westward to the transitional plains of San Juan, Parian, and Ambaley

(225,000 E, 1,640,000 N), channel density decreases, accounting for 30% of the network. The remaining 10% of the tributaries are concentrated in the downstream reaches near the primary outlet at the estuary between Barangay Baroro and Paratong in Bacnotan (222,000 E, 1,640,000 N).

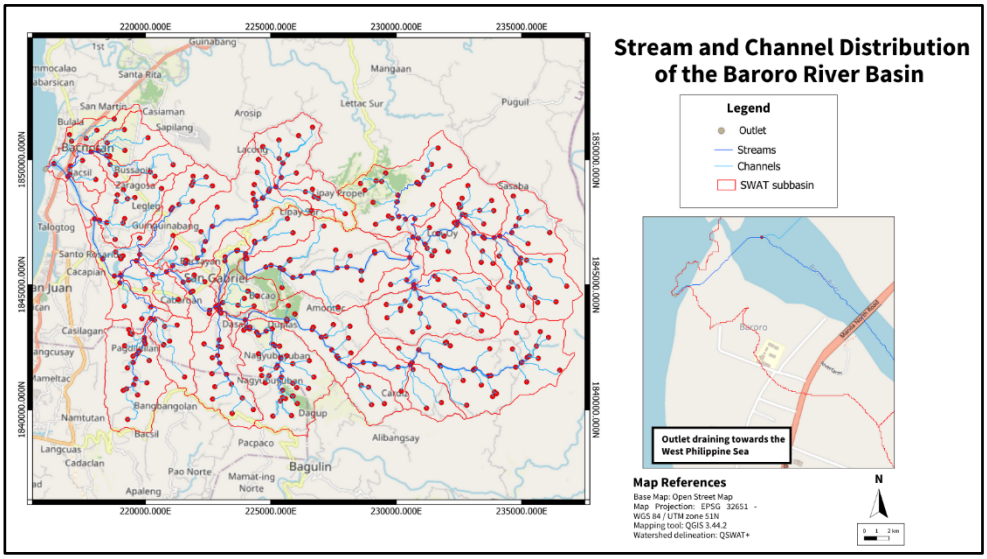

Figure 3. *Stream and Channel Distribution within the Baroro River Basin*

Stream hierarchy analysis follows the Strahler (1957) classification system, revealing a pyramidal structure consistent with Horton's law of stream numbers. As illustrated in Figure 4, the network is dominated by first-order headwater streams, which constitute 41.83% of the total channels. Subsequent orders decrease geometrically: second-order (29.09%), third-order (17.45%), and fourth-order (8.03%). The fifth-order mainstem, the Baroro River, represents only 3.6% of the distinct segments. This distribution reflects a typical bifurcation ratio for undisturbed terrains, facilitating efficient hydrological connectivity from headwaters to the coast.

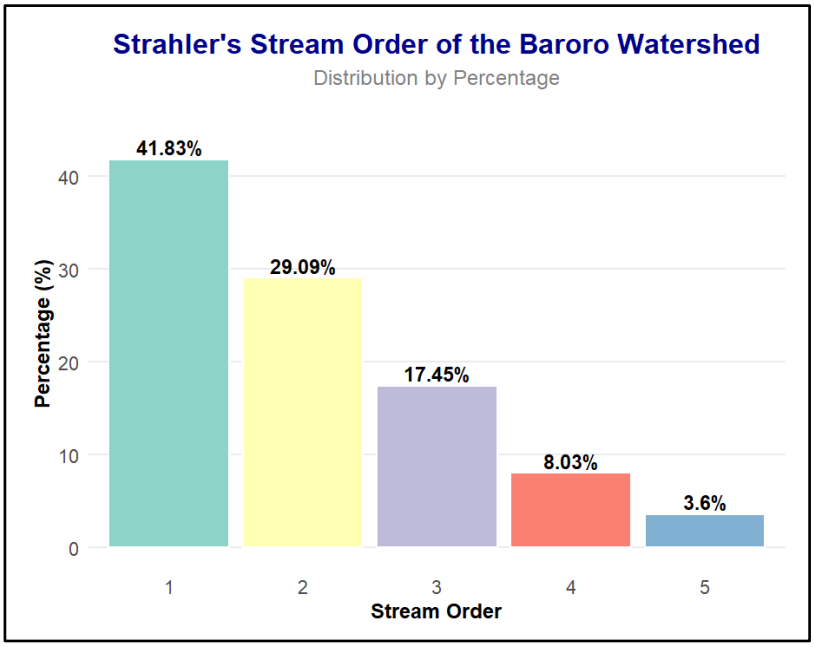

Figure 4. *Strahler's Stream Order Frequency Distribution of the Baroro Watershed*

Channel geometry metrics derived from the SWAT+ analysis are summarized in Table 3. Channel segment lengths exhibit a positively skewed distribution, with a mean length of 712.50 m, which is significantly higher than the median of 586.03 m. This skewness reflects the topographical contrast of the watershed: shorter, steeper tributaries

dominate the upstream Cordillera region, while longer channel extents characterize the western lowland subbasins. The data show moderate variability (SD = 557.67 m), with most reaches clustering between 15 m and 1,300 m. The leptokurtic distribution (*Kurtosis* = 1.49) highlights a strong central tendency, with a pronounced elongation in the mainstem reaches.

Table 3. *Channel Length of Baroro Watershed Streams and Associated Tributaries (in meters)*

Channel Length (in m)	Frequency	Percent (%)
(5-348.43]	125	29.98%
(348.43-691.87]	118	28.30%
(691.87-1035.3]	87	20.86%
(1035.3-1378.73]	37	8.87%
(1378.73-1722.17]	22	5.28%
(1722.17-2065.6]	17	4.08%
(2065.6-2409.03]	6	1.44%
(2409.03-2752.47]	4	0.96%
(2752.47-3095.9]	1	0.24%

Land cover classification in the year 2020 retrieved from GeoPortal denominates the Baroro Watershed into the following categories: (i) forest-mixed, (ii) range-grasses, (iii) generic agricultural land, (iv) medium density urban, (v) barren land, (vi) water, and (vii) wetlands. QSWAT+ terrain apportionment reveals how the 19,432.50 ha of the lotic system is dominated by a forest-mixed landscape (approximately 12,692 ha; 65.30%), followed by agricultural land-generic (31.80%; 6,179 ha) and an urban patch (2.60%; 505 ha). Wetlands and range grass environments exhibit low cover (0.001-0.05%; 7 ha of the total landscape). Aquatic systems in the area (associated with lotic settings of the watershed) cover 170 hectares (0.90% of the total area).

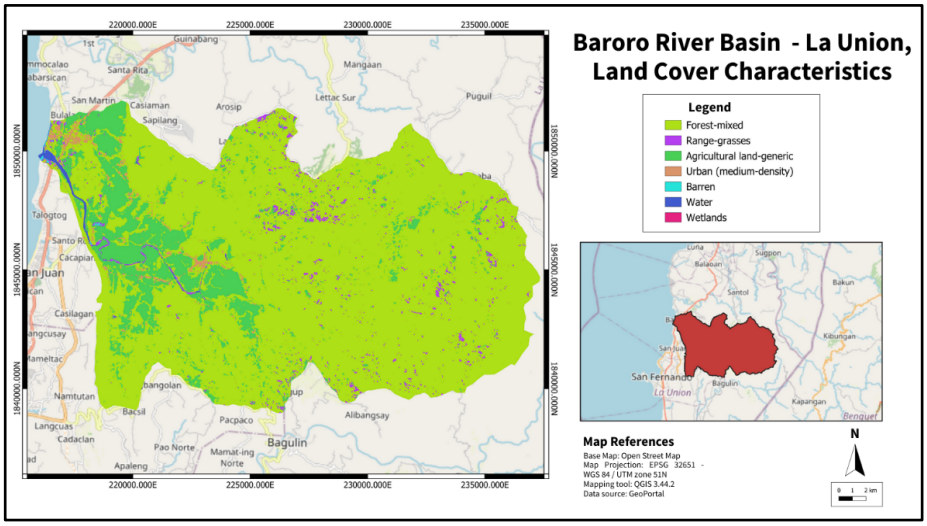

Figure 5. *Land Cover of the Baroro River Basin*

Pedo-Topographic Characteristics

Table 4. *Pedo-Topographic Characteristics of the Baroro River Basin*

Pedo-Topographic Variable	Unit	Mean	Median	Standard Deviation	Skewness	Kurtosis
Topographic Wetness Index	–	9.08	8.00	3.23	0.96	0.82
Soil Bulk Density	g/cm³	1.24	1.25	1.03	-1.59	1.62
Soil Water Potential	kPa	40.37	40.00	3.27	-1.95	27.84

The TWI of the Baroro River Basin exhibits a positive asymmetry, with a mean of 9.08 exceeding the median of 8.00. This distribution suggests that while the majority of the watershed (~60–70%) consists of well-drained slopes (*TWI* < 9), the hydrologic character is heavily influenced by clustered zones of saturation potential. The standard deviation of 3.23 further confirms that wetness is not uniformly distributed but rather concentrated in specific geomorphic features. Spatially, this is manifested as a prominent linear incision on the western flank, a 2-3 km wetness scar extending from mid-slopes (300 m elevation) toward the coastal outlets of San Juan (Figure 6-A).

Within this feature, TWI values range from 11 to 26, indicating a transition from transport zones to depositional basins, likely associated with alluvial fan formation (Reynolds et al., 2025).

The pedological footprint mirrors this hydrological gradient, as evidenced by the inverse relationship between BD and elevation. The watershed displays a pronounced leptokurtic distribution for BD (*Kurtosis* = 1.62), with a median ($\tilde{x}$ = 1.25 g/cm³) slightly surpassing the average ($\bar{x}$ = 1.24 g/cm³). This left-skewness (-1.59) is spatially driven by an erosion-deposition mechanism whereby upstream areas within the Cordilleras maintain lower densities (0–1.23 g/cm³) due to selective erosion, while downstream basins near the West Philippine Sea exhibit significantly higher compaction (1.27–1.49 g/cm³). This downstream densification aligns with the aforementioned alluvial scar, where the accumulation of mineralized sediments and fine silts has created a distinct pedological zone. Such environments facilitate compaction through aerobic conditioning and mineralization, establishing a structural foundation for the agricultural expanses identified in the overlay of Figures 6-A and 6-C.

SWP provides the capacity of soil to hold water. The metric displays exceptional statistical uniformity, characterized by extreme leptokurtosis (27.84) and a mean (40.37 kPa) that closely matches the median (40.00 kPa). This indicates that the vast majority of the watershed's 19,432.5 ha maintains moisture levels near field capacity (-40 kPa), likely buffered by the extensive mixed forest cover (65.3%). However, the negative skewness (-1.95) identifies a wetter tail of the distribution that corresponds precisely with the San Juan anomaly. In the vicinity of the topographic scar and high-density alluvial fan, SWP values drop to a range of 0–38 kPa. This convergence defines the area's high agroecological value: the alluvial fan acts as a nutrient sink with high BD and TWI, which helps the soil retain more water (closer to saturation) than the surrounding slopes. Consequently, the scar functions not merely as a drainage feature but also as a hydrologically subsidized storage house for alluvium and moisture, which are essential for the persistence of the observed riverine farm plots.

Relative to soil taxonomy, Table 5 depicts the soil taxon distribution in terms of hectare apportionment of the Baroro Watershed. It can be observed how Epiaquerts (30%) cover an approximate of 5,829.75 ha, followed by Haploxerolls (20%; 3,886.50 ha), and Ferrandals (15%; 2,914.88 ha). The heterogeneous pedological mosaic of Baroro implies a watershed with variable hydrologic responses. For instance, Epiaquert dominance in floodplains amplifies baseflow and nutrient export during wet seasons but risks erosion through episodes of gilgai microrelief, exacerbating sediment loads (De Benedetto et al., 2019). It is critical to recognize how Epiaquerts are a subgroup of Vertisols characterized by aquic moisture regimes, typically occurring in landscapes with seasonal water saturation (Di Bene et al., 2022). These soils are predominantly clay-rich, with heavy clay textures (often 30–95% clay fraction), dominated by smectite minerals that constitute the primary clay component, sometimes exceeding 30% of the soil and up to 98% in the clay fraction (Ferguson et al., 2020; Kovda et al., 2017). It is important to acknowledge how Epiaquerts often exhibit perched water tables, especially in lowlands, resulting in poor drainage, superficial saturation, and gleyic horizons during wet seasons (Di Bene et al., 2022).

Table 5. *Soil Taxonomic Distribution in the Baroro Watershed*

Soil Taxon	Percentage	Hectares
Epiaquerts	30	5,829.75
Haploxerolls	20	3,886.50
Ferrandalfs	15	2,914.88
Fluviosols	10	1,943.25
Natraquolls	5	971.63
Kandiudalfs	5	971.63
Natrixerolls	3	582.98
Argixerolls	3	582.98
Aquands	3	582.98
Dystropepts	2	388.65
Vermustalfs	1	194.33
Glossudalfs	1	194.33
Hapludox	1	194.33
No Recorded Taxon	1	194.33

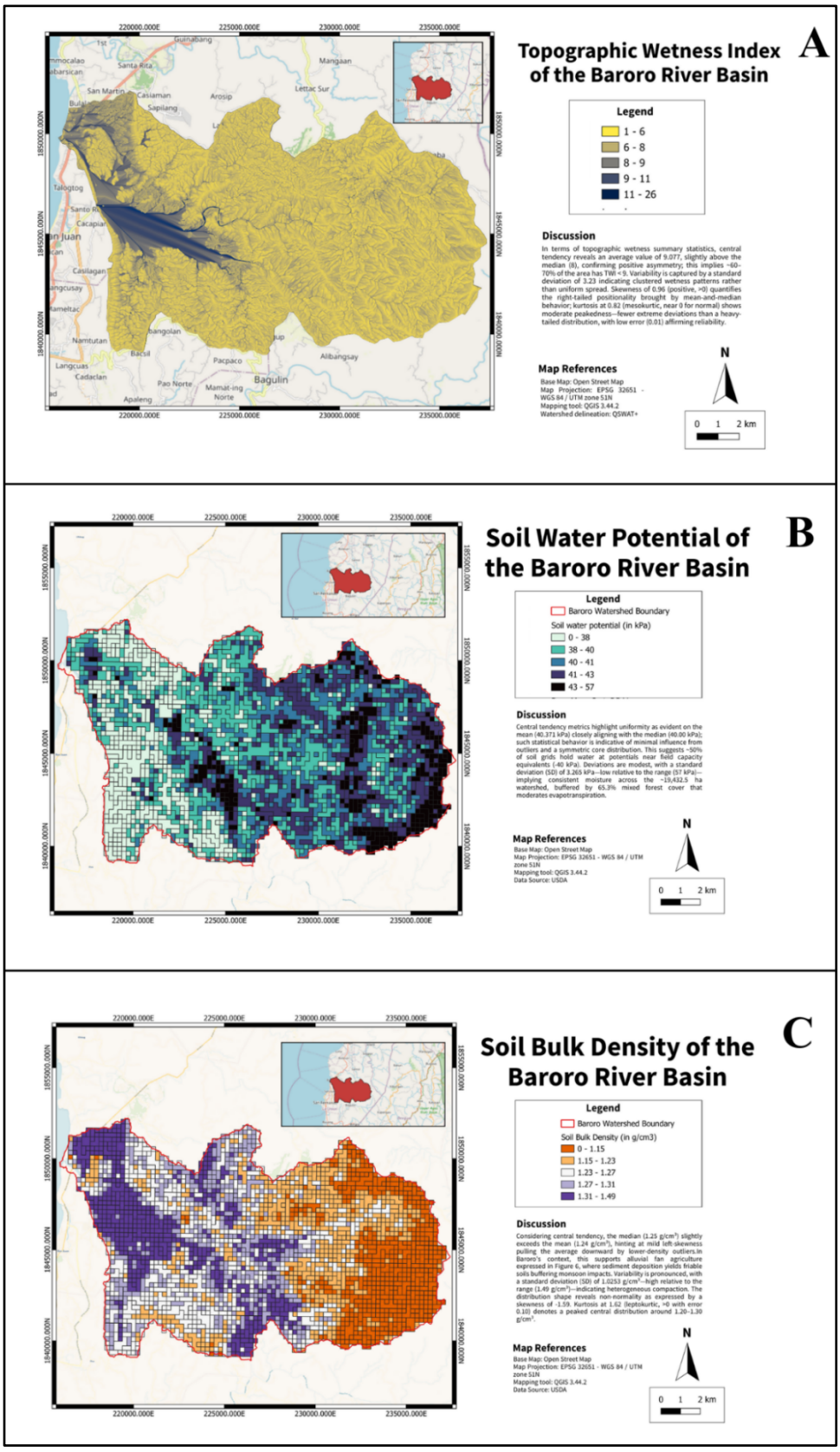

Figure 6. *Pedo-Topographic Characteristics of the Baroro River Basin: 6-A (Topographic Wetness Index), 6-B (Soil Water Potential), and 6-C (Soil Bulk Density)*

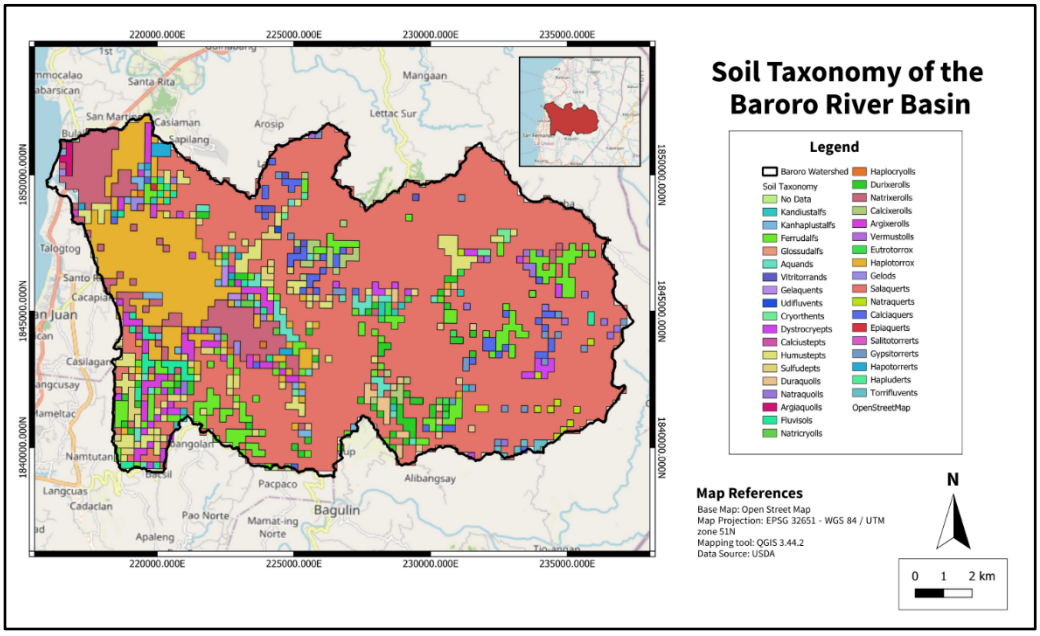

Figure 7. *Soil Taxonomy of the Baroro River Basin*

Soil-and-Hydrological Simulation

The simulation of the Baroro River Basin reveals a hydro-pedological trajectory characterized by distinct phases of stochastic oscillation and abrupt regime shifts. The time series data (1963–2063) elucidates the interplay between climatic variability and land surface modifications, highlighting the watershed's sensitivity to both meteorological extremes and theoretical land management interventions. The hydrological parameters, specifically rainfall and streamflow, exhibited high-frequency and amplitude-based fluctuations consistent with the Type I climate of the Ilocos Region (Tolentino et al., 2016). These oscillations are not uniform; they are punctuated by significant perturbations that align with historical meteorological records. Notable spikes in the observed flow and rainfall datasets correspond to periods of intensified cyclonic activity known to have devastated Northern Luzon. For instance, the dense clustering of peak discharge events observed in the late 2000s and 2010s strongly correlates with the onslaught of Typhoon Pepeng in 2009 and Typhoon Ompong in 2018. Such events underscore the basin's vulnerability to flash flooding and sediment transport, phenomena projected to persist well into the mid-21st century, as indicated by high-amplitude flow events modeled in the 2050s and 2060s (Abancó et al., 2021; Tolentino et al., 2016).

A divergence is observed between the observed and simulated flow regimes. While the observed data retain the erratic signature of extreme weather events, the simulated flow variable exhibits a dampened, rhythmic cyclicity. The persistence of discharge peaks in the latter half of the simulation implies a climate scenario where wet seasons intensify, a projection consistent with broader climate change assessments for the Philippine archipelago (Sangelantoni et al., 2019; Tolentino et al., 2016). This hydrological volatility necessitates a robust evaluation of the watershed's physical capacity to regulate flow, directing attention to the pedological underpinnings of the basin. In contrast to the stochastic nature of hydrological variables, pedological parameters exhibit a distinct, monotonic regime shift beginning in the early 21st century. Historically, bulk density values ranged between 1.2 and 1.6 g/cm^3, indicative of mineral soils in mixed-use or agricultural landscapes. The simulation reveals a precipitous decline in BD, beginning around 2005–2010, that stabilizes at remarkably low values (~0.4 g/cm^3) by the 2030s. Concurrently, SWP values drop from a historical range of 40–50 kPa to near-saturation levels (~10 kPa). This inverse relationship indicates a transition toward highly porous media with enhanced water retention capacities. In the context of the Baroro River Basin, where forest fragmentation has historically been documented (Encisa-Garcia et al., 2020), this trend does not reflect a business-as-usual pattern of urbanization. Urban expansion, particularly in downstream municipalities like San Juan, typically results in soil compaction and increased imperviousness. Therefore, the modeled reduction in bulk density is interpreted here as a normative restoration scenario, simulating the aggressive reversion of compacted agricultural lands to protected forest zones, thereby increasing soil organic carbon and porosity (Cruz et al., 2014).

The implications of these trends are critical for ecosystem service valuation. The anomaly observed in the TWI, specifically the crash to near-zero values in the late 1970s, suggests drastic changes in flow-accumulation paths, possibly due to infrastructure interventions. The overarching trend of improved soil structure and moisture retention implies a theoretical enhancement of the watershed's regulating services. By increasing the basin's sponge effect, the restored soil profile portrayed in the simulation would theoretically mitigate the flash-flood risks associated with the aforementioned typhoons. This highlights the divergence between the current reality of urban expansion and the necessary ecological interventions. While rapid land-use changes in San Gabriel and San Juan threaten to exacerbate runoff (Ramirez et al., 2019), the simulation provides a quantitative assessment of the hydrological benefits achievable through rigorous watershed zoning and reforestation efforts.

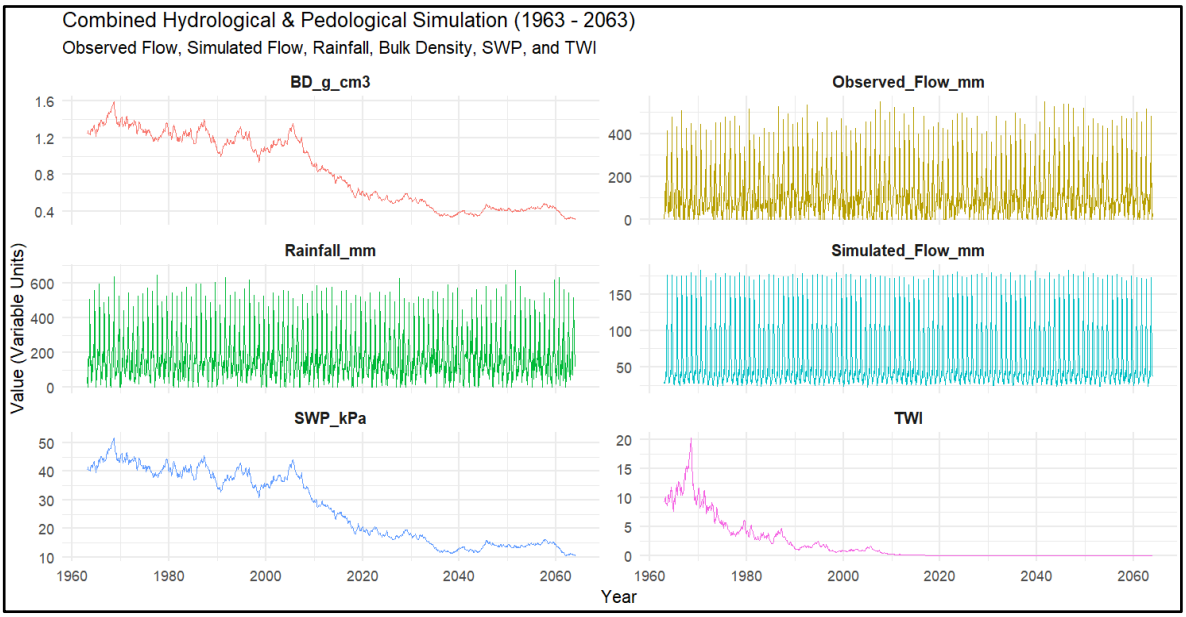

Figure 8. *Combined Hydrological and Pedological Simulation (1963 - 2063)*

The statistical characterization of hydro-meteorological variables in the Baroro River Basin revealed a distinct decoupling between precipitation inputs and hydrological response. As detailed in Table 6, rainfall events exhibited a high average intensity ($\bar{x}$ = 90.35 mm) with a negative skewness, indicating that while average precipitation is substantial, the distribution is weighted towards larger, less frequent storm events. This high-energy input, however, undergoes significant attenuation as it translates into streamflow. Observed flow ($\bar{x}$ = 65.60 m^3/s) is notably lower than rainfall inputs, a reduction that becomes even more pronounced in the simulated flow values ($\bar{x}$ = 29.58 m^3/s). This damping effect, in which simulated discharge is roughly 45% of observed flow, suggests a watershed with high abstraction capacity, with canopy interception and soil infiltration buffering storm runoff (Nainar et al., 2021; Nowak & Greenfield, 2018). The observed and simulated flows showed negative kurtosis (-3.08 and -2.54, respectively), implying that the watershed's discharge regime is relatively consistent, dominated by baseflow or moderate flow events rather than flashy, extreme peaks. The alignment of negative skewness across rainfall (-0.48) and flow (-0.37 observed) further corroborates a system in which extreme low-flow or dry periods are rare, likely sustained by the region's localized convective rainfall patterns or persistent subsurface drainage (Armstrong et al., 2008; Olden & Poff, 2003).

Table 6. *Measures of Spread and Central Tendency on Simulated Hydro-Meteorological and Pedo-Topographic Variables*

Variable	Unit	Mean	Median	Standard Deviation	Skewness	Kurtosis
Rainfall	mm	90.35	136.04	80.54	-0.48	-3.09
Observed Flow	m^3/s	65.60	83.76	58.14	-0.37	-3.08
Simulated Flow	m^3/s	29.58	39.52	25.13	-0.23	-2.54
Soil Water Potential	g/cm^3	13.59	12.34	13.22	0.11	-2.98
Soil Bulk Density	kPa	0.69	0.81	0.48	0.14	-0.33
Topographic Wetness Index	–	1.98	0.13	3.47	2.27	8.03

The interaction between soil structure and moisture retention offers a physical explanation for the observed flow dampening. Soil BD presents an average of ($\bar{x}$ = 0.69 g/cm³), a value significantly lower than that of typical mineral soils 1.3–1.5 g/cm³). This low density, combined with the median (0.81 g/cm³), points to highly porous, organic-rich soils typical of forest floors or uncompacted upland slopes. The negative kurtosis (-0.33) suggests a broad, uniform spread of density values across the watershed, avoiding concentration around a single mean. Hydrologically, this high porosity facilitates rapid infiltration, thereby reducing immediate surface runoff and contributing to the observed flow attenuation. Conversely, SWP exhibits a positive skewness and a mean ($\bar{x}$ = 13.59 kPa) close to its median ($\tilde{x}$ = 12.34 kPa). These values, near field capacity, indicate that the watershed's soils are in a state of persistent energetic equilibrium, rarely drying out completely or remaining fully saturated. This consistent moisture availability supports the earlier hypothesis of sustained baseflow.

TWI is the only terrain variable with extreme values for asymmetry (*Skewness* = 2.27) and leptokurtosis (*Kurtosis* = 8.03). While the median TWI is low (0.13), the high mean ($\bar{x}$ = 1.98) and standard deviation (*SD* = 3.47) are driven by a long right tail of extreme wetness values. This statistical signature confirms that, while most of the Baroro landscape consists of well-drained, steep terrain, there are distinct, spatially concentrated zones of extreme saturation, as evidenced by the identified alluvial fans and riparian corridors in previous sections. These high-TWI hotspots act as critical hydrological capacitors, accumulating runoff from the steep, low-density slopes and maintaining the localized saturation necessary for the region's agricultural persistence.

Hydro-Meteorological Correlations and Pedo-Topographic Regimes

The correlation analysis of the Baroro Watershed's hydro-meteorological and pedological variables, spanning a century-scale simulation (1963–2063b), reveals a system defined by two distinct statistical regimes: a highly responsive temporal domain governed by precipitation dynamics, and a rigidly structured spatial domain defined by landscape and soil properties. As illustrated in the pairwise relationship matrix and correlation summaries (Figure 9), the watershed exhibits strong internal coherence within these groups, while maintaining statistical independence between them. The following sections interpret these associations, distinguishing between the fluid dynamics of flow generation and the static architecture of the catchment.

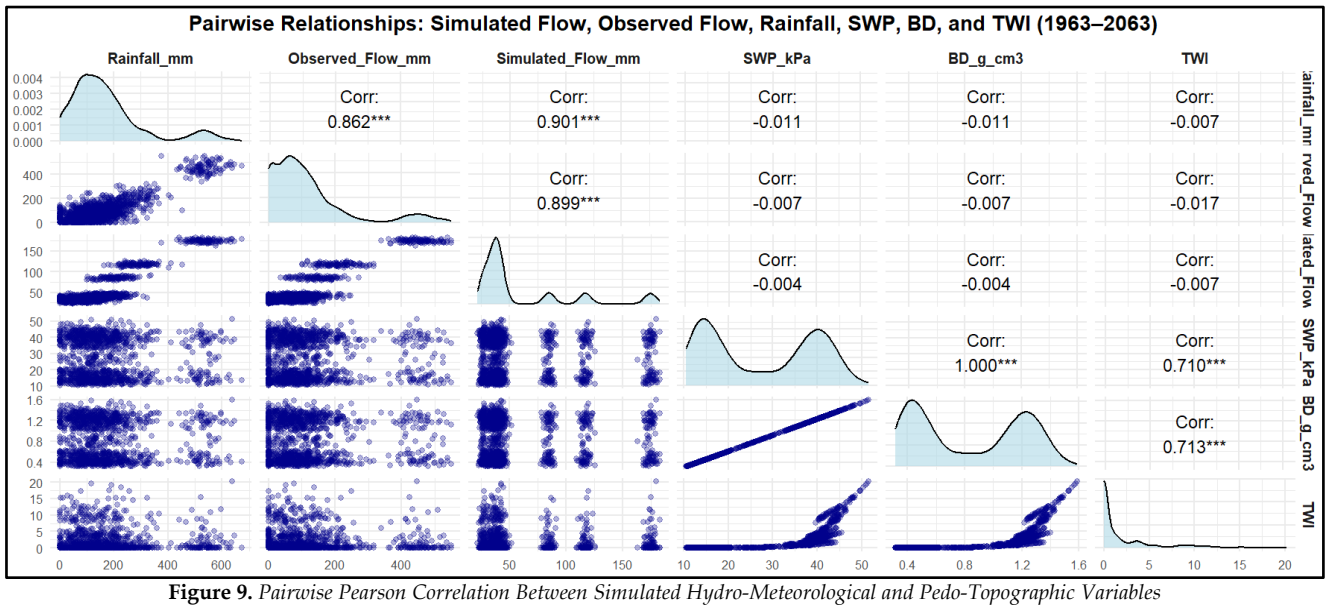

Figure 9. *Pairwise Pearson Correlation Between Simulated Hydro-Meteorological and Pedo-Topographic Variables*

A strong linear relationship between atmospheric inputs and discharge characterizes the hydrological behavior of the Baroro Watershed. Rainfall demonstrates a strong, significant positive correlation with Observed Flow (r = 0.862, p < 0.001) and an even stronger association with Simulated Flow (r = 0.901, p < 0.001). Statistically, such a degree of synchronicity suggests a catchment with high hydraulic connectivity, where precipitation inputs are rapidly translated into channel runoff rather than being significantly delayed by deep storage or lag times (Jencso et al., 2009). The scatter plots for these relationships clearly display this positive trend. This pattern is typical of tropical watersheds, where saturation-excess overland flow mechanisms become dominant during high-intensity storm events, engaging a larger fraction of the watershed in runoff generation than during low-intensity events.

The correlation between Observed Flow x Simulated Flow is notably significant ($r = 0.899$, $p < 0.001$). This statistical nuance suggests that the simulation may slightly idealize the rainfall-runoff transformation, potentially smoothing out some of the variability in interception loss and preferential flow paths (Bonell, 1993; Campling et al., 2002). The convergence of these metrics confirms that the temporal variability of the Baroro River Basin is driven by meteorological forcing rather than by internal state changes.

In contrast to the dynamic flux of water, the soil and topographic variables (SWP, BD, TWI) form a tightly coupled structural cluster that defines the watershed's physical template. A striking feature of this analysis is the perfect linear correlation ($r = 1.000$, $p < 0.001$) between SWP and BD. In physical hydrology, SWP is typically a function of moisture content and pore structure; however, a perfect correlation of unity strongly implies a structural coupling in the dataset's parameterization. It suggests that within the modeled environment, the energetic state of soil moisture (SWP) is fundamentally determined by the soil's physical compaction (BD). This density-potential lock indicates that as soil compaction increases, which reduces pore space, the matric forces governing water retention scale linearly (Goldberg-Yehuda et al., 2024). This finding highlights the critical role of soil structure in defining the watershed's storage capacity, as variations in bulk density are not merely physical attributes but direct proxies for the hydrological energy baseline of the soil matrix (Liu et al., 2024).

Extending this structural analysis to the landscape scale, both SWP and BD exhibit strong positive correlations with the TWI, with coefficients of ($r = 0.710$ and $r = 0.713$), respectively. The TWI is a geomorphic metric that identifies areas prone to saturation (typically valley bottoms and convergent slopes). A positive correlation here indicates that as one moves towards these convergent, wetter zones, the BD and SWP values also tend to increase (Sørensen et al., 2006; Mousavi et al., 2022). This statistical alignment mirrors the geomorphic processes of erosion and deposition discussed in previous sections. In many watersheds, high-elevation slopes are characterized by coarser, well-drained, and often organic-rich soils with lower bulk density. Conversely, lowland valleys and depositional fans accumulate fine sediments, silts, and mineralized alluvium that naturally pack at higher densities. The data confirm this catena sequence. The wetness scars and alluvial fans identified in the spatial analysis are not only topographic depressions but also zones of distinct pedological densification (Abate & Kibret, 2016; Aweto & Enaruvbe, 2010). This downstream increase in BD x TWI ($r = 0.713$) suggests that the capacity of the Baroro River Basin to retain moisture is physically reinforced by the tighter soil structure found in its depositional zones. Thus, wet areas of the Baroro are not defined solely by slope convergence but also by a concurrent shift in soil texture and density that physically favors water retention (Souza & Almedia, 2025).

A critical observation from the pairwise matrix is the near-zero correlation between the hydro-meteorological group and the pedo-topographic cluster. For instance, precipitation shows negligible correlation with BD ($r = -0.011$) and TWI ($r = -0.007$). This statistical decoupling is expected and validates the independence of such terrain dimensions. Rainfall and flow (both observed and simulated) are dynamic, time-variant fluxes that vary hourly or daily. In contrast, BD and TWI are static or quasi-static spatial properties that remain constant over the simulation period (Addor et al., 2017). The absence of correlation suggests that the state of the Baroro River Basin's pedo-topographic characteristics does not fluctuate in direct synchrony with the forcing of precipitation events. Instead, the soil and topography serve as the fixed stage on which the dynamic play of rainfall and runoff unfolds. Although they do not correlate temporally, their influence is implicit: the strong correlation between rainfall and flow is moderated by these static parameters (Wagener et al., 2007).

Diagnostic Checks

The long-term simulation demonstrated exceptional model performance, achieving an NSE of 0.99. This significantly exceeds the threshold for 'good' performance (>0.65), indicating that the model captures over 98% of observed flow variability. In contrast to the calibration phase ($NSE = 0.39$), the long-term simulation benefited from averaged realizations, which effectively smoothed parameter uncertainties. Similarly, KGE improved from 0.67 during calibration to 0.919 in the long-term analysis. This high KGE reflects a linear correlation, near-unity variability, and minimal bias, suggesting effective parameterization over extended horizons where soil moisture carryover and land-use effects stabilize.

PBIAS shifted from a +9.8% overestimation during calibration to -4.5% in the long-term simulation. This value falls within the 'good' range (<10%), with the slight underestimation likely attributable to conservative runoff generation in the forested areas of the 19,364 ha watershed. Absolute error metrics further corroborated this stability; the RMSE of 12.82 mm and MAE of 9.88 mm were minimal relative to peak flows (~500 mm). The RMSE,

in particular, was less than half the calibration value (29.43 mm), confirming reduced volatility and satisfying SWAT guidelines for monthly simulations (Moriasi, 2007; Arnold et al., 2012).

Table 7. *Diagnostic Checks on SWAT Hydrological Simulation*

Pedo-Topographic Variable	Long-Term	Calibrated
Nash-Sutcliffe Efficiency (NSE)	0.99	0.39
Kling-Gupta Efficiency (KGE)	0.92	0.67
Percent Bias (PBIAS)	-4.50%	9.80%
Mean Absolute Error (MAE)	9.88	23.08
Root Mean Square Error (RMSE)	12.82	29.43

Table 8. *Diagnostic Checks on Pedo-Topographic Variables Under a Geometric Brownian Motion*

Pedo-Topographic Variable	Theoretical σ	Estimated σ	Empirical Standard Deviation	Normality p-value
SWP	0.09	0.08	< .001	0.981
BD	0.08	0.08	< .001	0.970
TWI	0.36	0.33	0.019	0.957

The fundamental distributional assumptions of the Geometric Brownian Motion process were verified using normality tests on the log-returns of the simulated paths. The lag-1 autocorrelation was observed to be effectively at zero, demonstrating model consistency. The resulting p-values for all variables were high: 0.981 for SWP, 0.970 for BD, and 0.957 for TWI, which satisfy the normality condition under the Kolmogorov-Smirnov test. This statistical evidence fails to reject the null hypothesis, thereby confirming that the simulated temporal evolution of these landscape features follows a log-normal distribution. The extremely low empirical standard deviations indicate that the generated shocks ensured that the long-term simulation reflected realistic landscape resilience rather than chaotic variance.

Conclusion

The research synthesis confirms that the Baroro River Basin is not merely a passive channel for water transport but a dynamic, heterogeneous system defined by distinct feedback loops between its geomorphology and its inhabitants. The SWAT+ delineation and subsequent statistical analysis have exposed a fundamental decoupling between the basin's dynamic meteorological inputs and its static physical architecture.

A pivotal finding of this study is the identification of the structural lock between SWP, SBD, and TWI. The strong statistical association (r = 2) between SWP and BD indicates that the watershed's capacity to regulate water is intrinsically linked to land-surface modification. The simulation data (1963–2063) provide a stark counter-narrative to current urbanization trends; it models a restoration scenario in which bulk density decreases to 0.4 g/cm³, mimicking a return to forest cover. This contrasts sharply with the reality of urban sprawl in San Juan and San Gabriel, which drives soil compaction and increases impervious surface area.

The discovery of the San Juan Wetness Scar, a 2–3 km zone of high TWI and sediment accumulation, redefines the understanding of the basin's agricultural resilience. This alluvial fan acts as a hydrological capacitor, subsidized by upstream erosion to maintain the moisture and nutrient levels necessary for the persistence of riverine farm plots. However, this resilience is fragile. The decline in rice and corn yields, despite stable habitat quality, suggests that the trade-offs between bioproduction and ecosystem services are becoming unsustainable. In conclusion, the Baroro River Basin is a system with high hydraulic connectivity but diminishing regulatory capacity. The historic conversion of forest lands to agriculture has fragmented the landscape, stripping away the sponge effect needed to buffer the region's high-intensity rainfall. Without intervention, the trajectory points toward increased flash flood risks, loss of carbon storage, and the destabilization of the food-water nexus.

To bridge the divergence between the simulated restorative potential and the prevailing reality of watershed degradation, a multi-phased management framework is proposed. In the immediate term (0–3 years), priority must be placed on safeguarding the San Juan Anomaly, a critical zone of hydrological storage and alluvial deposition. To prevent the permanent loss of this natural drainage feature to urbanization, municipal Comprehensive Land Use Plans (CLUPs) should strictly zone these high-wetness areas for sustainable agriculture rather than built-up infrastructure. Concurrently, the strong statistical correlation between rainfall and discharge (r = 0.901) underscores the vulnerability to flash flooding and necessitates deploying a community-based hydro-

meteorological network. Installing cost-effective precipitation and stream sensors in the headwaters of Bagulin and San Gabriel is essential for feeding real-time data into a localized Early Warning System (EWS) for downstream communities. Furthermore, to mitigate erosion that drives downstream soil densification, agricultural extension programs should aggressively promote contour farming and cover cropping in transitional mid-slope zones.

Over the longer term, restoration strategies must pivot from superficial planting metrics to deep pedological rehabilitation. Reforestation efforts in the Cordillera foothills should prioritize native species that enhance soil porosity, with the explicit goal of lowering BD to the simulated target of <1.0 to restore infiltration and carbon storage capacity. To sustain these ecological services, a Payment for Ecosystem Services (PES) mechanism should be implemented, allowing downstream beneficiaries in San Fernando City and San Juan to compensate upstream stewards financially for forest maintenance—a strategy aligned with local livelihood needs (Ramirez et al., 2022). Effective governance requires transcending administrative borders by establishing a transboundary Baroro River Basin Management Council. This body should utilize the established SWAT+ and GIS baselines to guide policy, enforce limits on forest fragmentation, and manage the six municipalities as a single, functional hydro-ecological unit.

Contributions of Authors

Jericho A. Trio: simulations, QGIS mapping, conceptualization
Patricia Mae M. Clariño: discussion, review of related literature
Chris C. Guevarra: discussion, review of related literature

Funding

This research received no financial aid or funding from any institutions.

Conflict of Interests

The authors of the paper declare no conflict of interest.

Acknowledgment

The researchers of the study would like to acknowledge the School of Environmental Science and Management (SESAM) and the College of Human Ecology (CHE) in the University of the Philippines Los Baños for their support and guidance in this endeavor. This research is dedicated to all environmental planners, human ecologists, and environmental scientists who, in their efforts, sought a context-based, evidence-driven management of natural resources, particularly watershed areas, in the Philippines.

References

Abancó, C., Bennett, G., Matthews, A., Matera, M.A., & Tan, F. (2021). The role of geomorphology, rainfall and soil moisture in the occurrence of landslides triggered by 2018 Typhoon Mangkhut in the Philippines. Natural Hazards and Earth System Sciences, 21(5), 1531–1550. https://doi.org/10.5194/nhess-21-1531-2021

Abate, N., & Kibret, K. (2016). Effects of land use, soil depth and topography on soil physicochemical properties along the toposequence at the Wadla Delanta Massif, Northcentral Highlands of Ethiopia. Environment and Pollution, 5(2), 57. https://doi.org/10.5539/ep.v5n2p57

Addor, N., Newman, A., Mizukami, N., & Clark, M. (2017). The CAMELS data set: Catchment attributes and meteorology for large-sample studies. Hydrology and Earth System Sciences, 21(10), 5293–5313. https://doi.org/10.5194/hess-21-5293-2017

Allen, E. (2007). Modeling with Itô Stochastic Differential Equations. Dordrecht: Springer Netherlands.

Almarines, N., Hashimoto, S., Pulhin, J., Predo., C., Pulhin, F., Magpantay, A., & Saito, O. (2024). Spatiotemporal dynamics of bioproduction systems and ecosystem services in the Baroro and Pagsanjan-Lumban watersheds, Philippines. Paddy and Water Environment, 23(2), 277–300. https://doi.org/10.1007/s10333-024-01015-2

Aloui, S., Mazzoni, A., Elomri, A., Aouissi, J., Boufekane, A., & Zghibi, A. (2023). A review of Soil and Water Assessment Tool (SWAT) studies of Mediterranean catchments: Applications, feasibility, and future directions. Journal of Environmental Management, 326, 116799. https://doi.org/10.1016/j.jenvman.2022.116799

Arkhangelskaya, T., & Lukyashchenko, K. (2018). Estimating soil thermal diffusivity at different water contents from easily available data on soil texture, bulk density, and organic carbon content. Biosystems Engineering, 168, 83–95. https://doi.org/10.1016/j.biosystemseng.2017.06.011

Armstrong, D., Parker, G., & Richards, T. (2008). Characteristics and classification of least altered streamflows in Massachusetts. Scientific Investigations Report. https://doi.org/10.3133/sir20075291

Arnold, J.G., Moriasi, D.N., Gassman, P.W., Abbaspour, K.C., White, M.J., Srinivasan, R., & Jha, M.K. (2012). SWAT: Model use, calibration, and validation. Transactions of the ASABE, 55(4), 1491–1508.

Aweto, A., & Enaruvbe, G. (2010). Catenary variation of soil properties under oil palm plantation in South Western Nigeria. Ethiopian Journal of Environmental Studies and Management, 3(1). https://doi.org/10.4314/ejesm.v3i1.54389

Beven, K.J., & Kirkby, M.J. (1979). A physically based, variable contributing area model of basin hydrology. Hydrological Sciences Bulletin, 24(1), 43–69. https://doi.org/10.1080/02626667909491834

Bonell, M. (1993). Progress in the understanding of runoff generation dynamics in forests. Journal of Hydrology, 150(2–4), 217–275. https://doi.org/10.1016/0022-1694(93)90112-m

Box, G.E., Jenkins, G.M., Reinsel, G.C., & Ljung, G.M. (2015). Time series analysis: Forecasting and control. John Wiley & Sons.

Bressloff, P. (2024). Generalized Itô's lemma and the stochastic thermodynamics of diffusion with resetting. Journal of Physics A: Mathematical and Theoretical, 57(44), 445003. https://doi.org/10.1088/1751-8121/ad8495

Campling, P., Gobin, A., Beven, K., & Feyen, J. (2002). Rainfall-runoff modelling of a humid tropical catchment: The TOPMODEL approach. Hydrological Processes, 16(2), 231–253. Portico. https://doi.org/10.1002/hyp.341

Chawanda, C.J., George, C., Thiery, W., van Griensven, A., Tech, J., Arnold, J., & Srinivasan, R. (2020). User-friendly workflows for catchment modelling: Towards reproducible SWAT+ model studies. Environmental Modelling & Software, 134, 104812. https://doi.org/10.1016/j.envsoft.2020.104812

Crow, W., Berg, A., Cosh, M., Loew, A., Mohanty, B., Panciera, R., de Rosnay, P., Ryu, D., & Walker, J. (2012). Upscaling sparse ground-based soil moisture observations for the validation of coarse-resolution satellite soil moisture products. Reviews of Geophysics, 50(2). Portico. https://doi.org/10.1029/2011rg000372

Cruz, R.V., Carandang, W.M., Carandang, V.Q., de Luna, C.C., & Galapia, G.A. (2014). Collaborative monitoring system for enhanced watershed management: The case of the Baroro Watershed in La Union, Philippines (CBA2014-03NSY-Cruz). Asia-Pacific Network for Global Change. https://tinyurl.com/bdwkpcjn

De Benedetto, D., Montemurro, F., & Diacono, M. (2019). Mapping an agricultural field experiment by electromagnetic induction and ground penetrating radar to improve soil water content estimation. Agronomy, 9(10), 638. https://doi.org/10.3390/agronomy9100638

de Souza, A.P., & de Almeida, F. T. (2025). The effect of land use and management on soil properties and processes. Soil Systems, 9(2), 54. https://doi.org/10.3390/soilsystems9020054

Di Bene, C., Diacono, M., Montemurro, F., Testani, E., & Farina, R. (2022). EPIC model simulation to assess effective agro-ecological practices for climate change mitigation and adaptation in organic vegetable system. Agronomy for Sustainable Development, 42(1). https://doi.org/10.1007/s13593-021-00745-5

Encisa-Garcia, J., Pulhin, J., Cruz, R.V., Simondac-Peria, A., Ramirez, M.A., & De Luna, C. (2020). Land use/land cover changes assessment and forest fragmentation analysis in the Baroro River Watershed, La Union, Philippines. Journal of Environmental Science and Management, 14. https://doi.org/10.47125/jesam/2020_sp2/02

Ferguson, J.C., Krutz, L.J., Calhoun, J., Gholson, D., Merritt, L., Wesley, M., Jr., Broster, K., & Treadway, Z. (2020). Optimizing overhead irrigation droplet size for six Mississippi soils. Agronomy, 10(4), 574. https://doi.org/10.3390/agronomy10040574
Goldberg-Yehuda, N., Nachshon, U., Assouline, S., & Mau, Y. (2024). The effect of mechanical compaction on the soil water retention curve: Insights from a rapid image analysis of micro-CT scanning. CATENA, 242, 108068. https://doi.org/10.1016/j.catena.2024.108068
Gutmann, E., Pruitt, T., Clark, M., Brekke, L., Arnold, J., Raff, D., & Rasmussen, R. (2014). An intercomparison of statistical downscaling methods used for water resource assessments in the United States. Water Resources Research, 50(9), 7167–7186. Portico. https://doi.org/10.1002/2014wr015559
Herrera, P.A., Marazuela, M.A., & Hofmann, T. (2021). Parameter estimation and uncertainty analysis in hydrological modeling. WIREs Water, 9(1). Portico. https://doi.org/10.1002/wat2.1569
Hillel, D. (2003). Introduction to environmental soil physics. Elsevier.
Issac, J., & Newell, R. (2025). Integrating stakeholder knowledge through a participatory approach and semi-quantitative analysis for local watershed management. Systems, 13(5), 364. https://doi.org/10.3390/systems13050364
Jencso, K., McGlynn, B., Gooseff, M., Wondzell, S., Bencala, K., & Marshall, L. (2009). Hydrologic connectivity between landscapes and streams: Transferring reach- and plot-scale understanding to the catchment scale. Water Resources Research, 45(4). Portico. https://doi.org/10.1029/2008wr007225
Kovda, I., Goryachkin, S., Lebedeva, M., Chizhikova, N., Kulikov, A., & Badmaev, N. (2017). Vertic soils and Vertisols in cryogenic environments of Southern Siberia, Russia. Geoderma, 288, 184–195. https://doi.org/10.1016/j.geoderma.2016.11.008
Lahoti, S.A., Lomente-Gacutan, L.L., Cruz, R.V., Montoya, P., Magpantay, A., Sevilla, F., Sahle, M., Pulhin, J., Hashimoto, S., & Saito, O. (2025). Localizing visions of desirable futures: Applying the nature futures framework to the Baroro Watershed in the Philippines. Sustainability Science. https://doi.org/10.1007/s11625-025-01688-6
Lal, R. (2015). Restoring Soil quality to mitigate soil degradation. Sustainability, 7(5), 5875–5895. https://doi.org/10.3390/su7055875
Lee, C.-H., Lee, N., & Kim, J.-T. (2021). SWAT model calibration/validation using SWAT-CUP in Danjang-stream watershed. Journal of the Korea Academia-Industrial Cooperation Society, 22(9), 235–246. https://doi.org/10.5762/kais.2021.22.9.235
Lillesand, T., Kiefer, R.W., & Chipman, J. (2015). Remote sensing and image interpretation. John Wiley & Sons.
Liu, Q., Guo, L., Miao, J., Guo, S., & Shu, J. (2024). Approaches for predicting the soil-water characteristic curves of compacted quartz sand based on particle packing theory. Scientific Reports, 14(1). https://doi.org/10.1038/s41598-024-73821-x
Moriasi, D.N., Arnold, J.G., Van Liew, M.W., Bingner, R.L., Harmel, R.D., & Veith, T.L. (2007). Model evaluation guidelines for systematic quantification of accuracy in watershed simulations. Transactions of the ASABE, 50(3), 885–900.
Mousavi, S.R., Sarmadian, F., Omid, M., & Bogaert, P. (2022). Three-dimensional mapping of soil organic carbon using soil and environmental covariates in an arid and semi-arid region of Iran. Measurement, 201, 111706. https://doi.org/10.1016/j.measurement.2022.111706
Nainar, A., Kishimoto, K., Takahashi, K., Gomyo, M., & Kuraji, K. (2021). How do ground litter and canopy regulate surface runoff?—A paired-plot investigation after 80 years of broadleaf forest regeneration. Water, 13(9), 1205. https://doi.org/10.3390/w13091205
Nowak, D., & Greenfield, E. (2018). US urban forest statistics, values, and projections. Journal of Forestry, 116(2), 164–177. https://doi.org/10.1093/jofore/fvx004
Olden, J., & Poff, N.L. (2003). Redundancy and the choice of hydrologic indices for characterizing streamflow regimes. River Research and Applications, 19(2), 101–121. Portico. https://doi.org/10.1002/rra.700
Park, S., Nielsen, A., Bailey, R., Trolle, D., & Bieger, K. (2019). A QGIS-based graphical user interface for application and evaluation of SWAT-MODFLOW models. Environmental Modelling & Software, 111, 493–497. https://doi.org/10.1016/j.envsoft.2018.10.017
Pulhin, F., Magpantay, A., Almarines, N., Predo, C., & Pulhin, J. (2024). Land cover change and carbon loss: A case study of the Pagsanjan-Lumban and Baroro watersheds in Luzon, Philippines. SciEnggJ, 17(Supplement), 268–280. https://doi.org/10.54645/202417suplof-25
Raghuwanshi, N.S., Singh, R., & Reddy, L.S. (2006). Runoff and sediment yield modeling using artificial neural networks: Upper Siwane River, India. Journal of Hydrologic Engineering, 11(1), 71–79. https://doi.org/10.1061/(asce)1084-0699(2006)11:1(71)
Ramirez, M.A., Pulhin, J., Garcia, J., Tapia, M., Pulhin, F., Cruz, R.V., De Luna, C., & Inoue, M. (2019). Landscape fragmentation, ecosystem services, and local knowledge in the Baroro River Watershed, Northern Philippines. Resources, 8(4), 164. https://doi.org/10.3390/resources8040164
Ramirez, M.A., Pulhin, J., & Inoue, M. (2022). Local people's perceptions of changing ecosystem services in Baroro River Watershed, Philippines. Grassroots Journal of Natural Resources, 05(01), 17–39. https://doi.org/10.33002/nr2581.6853.050102
Reynolds, S., Rohli, R.V., Johnson, J., Waylen, P., & Francek, M.A. (2025). Exploring physical geography (2nd ed.). McGraw-Hill Education.
Sangelantoni, L., Tomassetti, B., Colaiuda, V., Lombardi, A., Verdecchia, M., Ferretti, R., & Redaelli, G. (2019). On the use of original and bias-corrected climate simulations in regional-scale hydrological scenarios in the Mediterranean basin. Atmosphere, 10(12), 799. https://doi.org/10.3390/atmos10120799
Sammel, A., & McMartin, D. (2014). Teaching and knowing beyond the water cycle: What does it mean to be water literate? Creative Education, 05(10), 835–848. https://doi.org/10.4236/ce.2014.510097
Setegn, S., Srinivasan, R., & Dargahi, B. (2008). Hydrological modelling in the Lake Tana Basin, Ethiopia using SWAT model. The Open Hydrology Journal, 2(1), 49–62. https://doi.org/10.2174/1874378100802010049
Shawul, A.A., Alamirew, T., & Dinka, M.O. (2013). Calibration and validation of SWAT model and estimation of water balance components of Shaya mountainous watershed, Southeastern Ethiopia. https://doi.org/10.5194/hessd-10-13955-2013
Sørensen, R., Zinko, U., & Seibert, J. (2006). On the calculation of the topographic wetness index: Evaluation of different methods based on field observations. Hydrology and Earth System Sciences, 10(1), 101–112. https://doi.org/10.5194/hess-10-101-2006
Strahler, A. (1957). Quantitative analysis of watershed geomorphology. Transactions, American Geophysical Union, 38(6), 913–920. https://doi.org/10.1029/tr038i006p00913
Tolentino, P.L., Poortinga, A., Kanamaru, H., Keesstra, S., Maroulis, J., David, C.P., & Ritsema, C. (2016). Projected impact of climate change on hydrological regimes in the Philippines. PLOS One, 11(10), e0163941. https://doi.org/10.1371/journal.pone.0163941
Umar, M., Rhoads, B.L., & Greenberg, J. (2018). Use of multispectral satellite remote sensing to assess mixing of suspended sediment downstream of large river confluences. Journal of Hydrology, 556, 325–338. https://doi.org/10.1016/j.jhydrol.2017.11.026
Wagener, T., Sivapalan, M., Troch, P., & Woods, R. (2007). Catchment classification and hydrologic similarity. Geography Compass, 1(4), 901–931. Portico. https://doi.org/10.1111/j.1749-8198.2007.00039.x
Wohl, E. (2014). Rivers in the landscape: Science and management. Wiley-Blackwell.